Time-of-Flight Angiography

2

Seong-Eun Kim and Dennis L. Parker

Introduction

Time-of-flight (TOF) angiography is a widely used means of producing angiographic images without the need for the injection of contrast agent. In this chapter, we discuss the MR imaging (MRI) physics which governs the creation of TOF angiograms. We also describe the MRI pulse sequence used for TOF imaging, sources of artifact, and compensatory mechanisms to reduce the deleterious effect of these artifacts.

MR Signal in Time of Flight

The flow sensitivity of MRI methods is based on TOF effects, where the amplitude of the signal from flowing blood changes as it moves into the imaged volume, and phase effects, where motion of the blood during applied gradients results in a phase change due to motion. Both flow phenomena can be used to differentiate flowing spins from stationary spins by evaluating either the magnitude or the phase in the acquired MRI data.

TOF effects influence the signal intensities of moving blood in MR image in nonangiographic applications. For example, flow voids resulting from the motion through a slice- and flow-related enhancement (FRE) have commonly been seen in both spin echo and gradient echo imaging, respectively. TOF image contrast is based on establishing a difference in the longitudinal magnetization of moving spins relative to stationary spins. The TOF effect was first reported in a nonimaging application by Suryan [1] and in the imaging of blood vessels by Hinshaw et al. [2]. The magnetization of a bolus of flowing blood is typically modified at one location and detected a short time later at another location. Since time elapses between the modification and detection of the flowing magnetization, this effect is referred to as the "TOF" effect.

TOF techniques in MRA can be divided into those which yield a high signal from flowing spins and low signal from the background tissue (white blood) and those which yield strong signal from the background tissue and little signal from the flowing spins (black blood). White blood (sometimes called bright blood) techniques are the most commonly used for angiography and are the focus of the remainder of this chapter. In white blood TOF, static tissue is suppressed by using a spoiled gradient echo (SPGRE) sequence with relatively short TR. The spoiling suppresses (i.e., saturates) the signal from static tissue, and the TR is adjusted to be long enough so that a sufficient amount of blood can flow into the imaging plane creating contrast between flowing and static tissue.

TOF images can be acquired as two-dimensional (2D) or three-dimensional (3D) images. The acquisition of a 3D volume receives signal simultaneously from the entire volume of interest while a 2D acquisition receives signal sequentially from a series of image slices, one slice at a time. In both cases, images are stored as a 3D image dataset. For physician review, a projection angiogram from the 3D dataset is created by projecting the reconstructed image values through the 3D image volume, most commonly using the maximum intensity projection (MIP) [3]. 3D techniques in general have the advantage of higher signal-to-noise ratio (SNR) and higher spatial resolution than 2D techniques at the expense of lower blood vessel signal because the blood remains in the slab for a significant fraction of the imaging time. 2D TOF images generally have higher contrast between blood and background tissue than 3D techniques but have lower spatial resolution due to slice thickness larger than 2 mm. To reduce blood signal saturation while maintaining the SNR of 3D acquisition, Parker et al. [4] developed the multiple overlapping thin 3D slab acquisition (MOTSA) technique. MOTSA acquisitions have the high SNR typical of 3D acquisition with improved vessel contrast common to 2D acquisitions.

S.-E. Kim, PhD (✉) • D.L. Parker, PhD
Department of Radiology, Utah Center for Advanced Imaging Research, Salt Lake City, UT, USA
e-mail: sekim@ucair.utah.edu

J.C. Carr and T.J. Carroll (eds.), *Magnetic Resonance Angiography: Principles and Applications*,
DOI 10.1007/978-1-4419-1686-0_2,

The goal of TOF MRA is to provide an accurate depiction of the blood within the vascular lumen (artery or vein) noninvasively and various TOF techniques have been successful in meeting this challenge. The best results are achieved when appropriate pulse sequence parameters are matched to each clinical application. In some cases, alterations to the standard SPGR pulse sequence, such as the use of magnetization transfer (MT) saturation, flow compensation, MOTSA [5], or TONE [6], can improve diagnostic accuracy. In general, TOF MRA techniques are clinically useful in the evaluation of small aneurysms, atherosclerosis, vasospasm, and inflammatory vasculitis.

Quantification of the Time-of-Flight Effect

The TOF effect has been reviewed by Axel et al. [7], Gullberg et al. [8], and Nishimura [9] who modeled the signal on the basis of the Bloch equations for a variety of pulse sequence schemes for both plug and laminar flow. If the spins in stationary tissue experience a large number of RF pulses, the longitudinal magnetization of the stationary spins approaches a steady-state equilibrium value that is independent of position within the slice. However, when flowing spins, such as in blood, are flowing into and out of the slice, they may be subjected to fewer RF pulses resulting in a different steady-state magnetization.

In general, the TOF effect leads to a diminished blood signal in spin echo imaging. However, in gradient echo images with short TR, the TOF effect results in inflow signal enhancement, which increases the signal from flowing blood relative to static tissue. As a simplistic example, consider blood with plug flow, uniform velocity throughout the radius of the vessel, with speed v in a blood vessel with flow perpendicular to a slice to be imaged, as shown in Fig. 2.1. During the time, TR, between RF pulses, the fluid moves a distance, dz. Thus, in the time, TR, a length, dz, of nonexcited blood moves into the imaged slice. If dz is greater than slice thickness, z, the entire vessel segment within the slice is replaced by fresh inflowing blood shown as region *I* in Fig. 2.1a. If dz is less than z, then there will be sections of thickness dz that see one, then two, and three RF pulses as shown as region *I, II,* and *II*, respectively, in Fig. 2.1b. If the velocity of blood is exactly z/TR, the full slice thickness, $z = v\text{TR}$, will be completely replaced with fresh inflowing blood. The critical speed (2.1) is defined as:

$$V_c \equiv \frac{z}{\text{TR}}. \tag{2.1}$$

When the speed of blood is faster than V_c, the blood in the vessel that lies in the selected slice is completely refreshed by blood containing unsaturated spins. The fresh blood results in a higher signal relative to the stationary tissue signal since stationary tissue experiences many more RF pulses and is much more saturated. This effect is called wash-in, inflow enhancement or FRE. If $v < V_c$, partial saturation of the blood will begin to take place for distances into the slice greater than vTR. Fresh (fully magnetized) blood flowing into the imaging slice restores some of the signal intensity lost to partial saturation. In the simple example given above, the flow direction was perpendicular to the slice plane. Inflow enhancement of flow signal decreases for blood flow that transverses the blood vessel obliquely, and increases as

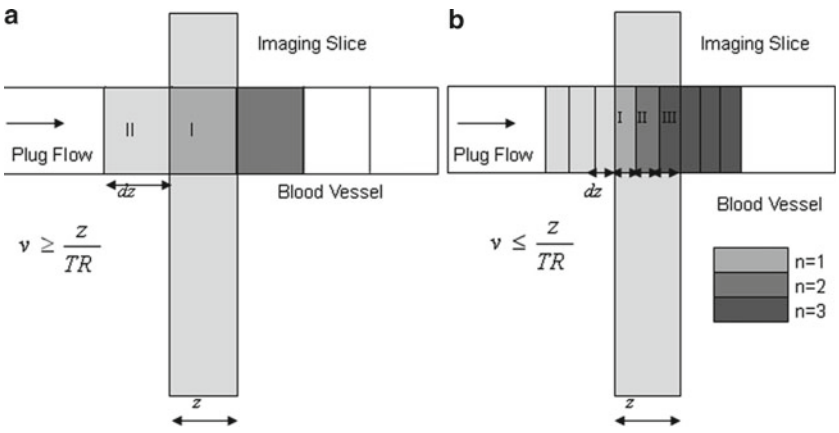

Fig. 2.1 TOF effects in the presence of plug flow with speed v in direction z. (**a**) When the velocity is higher than the critical velocity as given in (2.1), spins in the blood region I experience only one RF pulse and then exit the imaging slice before the next RF application. Spins in region II are not affected by the first excitation but by the next RF pulse. (**b**) When the blood is moving slower than the critical velocity, the saturation effect can be understood by dividing the slice into multiple segments. Blood located in each segment experiences a different number of RF pulses, RF(n), resulting in different saturation effects depending on n

the blood's speed increases above V_c. Inflow enhancement also increases as slice thickness is reduced since V_c is proportional to the slice thickness, z. If the perpendicular component of velocity exceeds the critical velocity, there is complete inflow replacement in the imaging slice during each TR. A further increase in velocity results in no further increase in blood signal enhancement and might even begin to decrease the signal due to intravoxel phase dispersion.

To extend this mathematical model to 3D TOF and MOTSA sequences, the slice thickness (z) can be replaced by the slab thickness, $N_z dz$. If the blood vessel is straight and perpendicular to the imaging slab, the critical velocity (2.2) is given by

$$V_c = \frac{N_z dz}{\mathrm{TR}} \tag{2.2}$$

and for velocities greater than the critical velocity, the blood inside the slab is completely replaced by fresh blood flowing from the outside of the slab.

For standard SPGR sequences, the TOF effect can be explained as the difference in signal saturation between flowing and static spins. Spins flowing into a slice may be less saturated than static spins resulting in angiographic contrast differences. The longitudinal magnetization of a stationary spin (i.e., after a series of RF pulses) with equilibrium magnetization, Mo, and longitudinal relaxation time, T1, subjected to the SPGR pulse sequence is given by [10]:

$$M_{z\,\mathrm{ss}} = \frac{M_0(1-\mathrm{e}^{-\mathrm{TR}/T_1})}{1-\mathrm{e}^{-\mathrm{TR}/T_1}\cos\theta}, \tag{2.3}$$

where θ is the flip angle and TR is the repetition time of the sequence, $T1$ is the longitudinal relaxation time of blood which is almost same as $T1$ of tissue, and M_0 is the equilibrium longitudinal magnetization. Before reaching the steady state, the longitudinal pulse (2.4) is given by:

$$M_z(n^-) = M_{z\,\mathrm{ss}} + (\mathrm{e}^{-\mathrm{TR}/T_1}\cos\theta)^{n-1}(M_0 - M_{z\,\mathrm{ss}})\, n \geq 1. \tag{2.4}$$

The transverse magnetization after the nth RF pulse (2.5) is given by

$$M_+(n) = M_z(n^-)\sin\theta \mathrm{e}^{-\mathrm{TE}/T_2}. \tag{2.5}$$

In cases when TR is much shorter than $T1$, as the number of RF pulses, n, increases, the contribution of the second term in (2.4) gets very small. Under these approximations, the transverse magnetization after the nth RF pulse (2.6) can be simplified as:

$$M_+ = \frac{M_0(1-\mathrm{e}^{-\mathrm{TR}/T_1})}{1-\mathrm{e}^{-\mathrm{TR}/T_1}\cos\theta}\sin\theta \mathrm{e}^{-\mathrm{TE}/T_2}. \tag{2.6}$$

As the TR/$T1$ ratio decreases, the transverse magnetization given in (2.6) monotonically decreases. In other words, saturation of the MRI signal increases. The maximum signal occurs when the flip angle is the Ernst angle ($\theta_E = \arccos(\exp(-\mathrm{TR}/T1))$, which implies that saturation is dominant over the creation of transverse magnetization for $\theta > \theta_E$. Inflowing fresh or fully magnetized blood entering into the imaging slice restores some of the signal intensity lost to partial saturation. Inflow enhancement increases with the blood velocity and as the imaging slice becomes perpendicular to the velocity direction. It also increases as slice thickness is reduced. As mentioned previously, if the perpendicular component of velocity exceeds the critical velocity, there is complete inflow replacement in the imaging slice during each TR. A further increase in velocity yields no further increase in the signal enhancement in blood and might even begin to decrease the signal due to intravoxel dephasing effects which are discussed in the next section.

When the blood experiences a single RF excitation pulse in an SPRE sequence, the amount of inflow enhancement in the spoiled gradient sequence is given by the difference (2.7):

$$M_+(n) - M_+ = M_0\sin\theta(\mathrm{e}^{-\mathrm{TR}/T_1}\cos\theta)^{n-1}\left(1-\frac{(1-\mathrm{e}^{-\mathrm{TR}/T_1})}{(1-\mathrm{e}^{-\mathrm{TR}/T_1}\cos\theta)}\right)\mathrm{e}^{-\mathrm{TE}/T_2^*}. \tag{2.7}$$

By using (2.7), the inflow enhancement effect can be simulated and quantified.

Figure 2.2 shows computer simulations based on (2.7). In these simulations, we studied how the normalized signal of the flow enhancement effect (FRE) changes as the flip angle (θ) increases for two cases: (a) $TR/T1 = 0.02$ and (b) when $TR/T1 = 0.1$. The normalized signal was obtained by dividing (2.6) by $M_0\mathrm{e}^{-\mathrm{TE}/T2^*}$. The simulation demonstrates that FRE increases as n decreases when the TR and slice thickness are fixed. For a fixed TR and slice thickness, increasing n means faster flow velocity. This trend continues until $v = V_{\max}$, at which point the flow experiences only one RF pulse and the flow enhancement effect reaches a maximum. If $n = 1$, the maximum transverse magnetization (2.8) is given by:

$$M_+(n=1) = M_0\sin\theta\mathrm{e}^{-\mathrm{TE}/T_2^*}. \tag{2.8}$$

Figure 2.2 shows that if there is no partial saturation ($n = 1$), the higher RF flip angle (90°) results in a maximum FRE. Comparing the curves, we see that the ratio of $TR/T1$ decreases and the flow enhancement intensity increases. When velocity v is smaller than the critical velocity, the flow enhancement effect can be modeled by subdivision of imaging slices into multiple compartments and summation of the geometric series shown in Fig. 2.1.

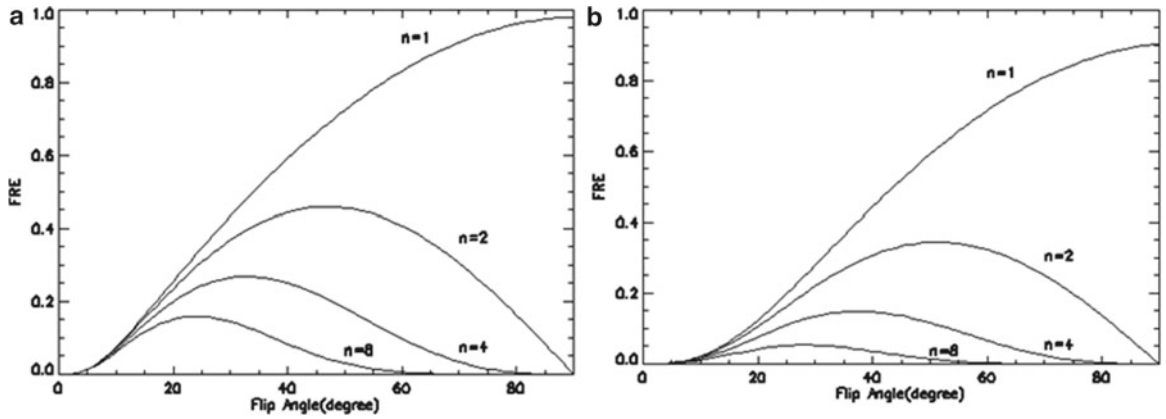

Fig. 2.2 Plots of the flow enhancement effect (FRE) simulated from (2.8). The label *n* is the number of excitation RF pulses experienced by spins located in the imaging slices

In general, arterial velocity is an interesting function of the branching nature of the vascular bed. From the aorta to the capillaries, as the vascular branches, the vessel cross-section becomes progressively smaller. However, the number of branches increases in such a manner that the total cross-section increases as the branching increases. Thus, from geometry alone, arterial velocity decreases with distance from the heart. In general, the velocity remains sufficiently high for successful inflow enhancement until diameters smaller than 0.2 mm are reached. For vessels that can be seen with TOF MRA, the velocities become relatively constant (less pulsatile) for the more distal segments.

Phase Dispersion and Flow Compensation

Signal intensity in MRI TOF imaging depends upon the imaging pulse sequence and the geometry and nature (velocity profile, pulsatility, etc.) of flow. Because of viscosity, flowing blood experiences frictional forces from the surrounding blood and vessel wall in addition to the force due to the pressure drop along the vessel. These forces generally result in a form of laminar flow. Laminar flow is characterized by a parabolic velocity profile, where the velocities in the center of the vessel are greater than those at the vessel wall. The magnetic field gradients used for spatial signal encoding in MRI impart a velocity-dependent phase at the time of signal acquisition. Because the velocity of blood varies considerably over dimensions that are much smaller than an image voxel, laminar flow can result in a range of phases for the signal generating spins within a voxel. If not properly compensated, this phase dispersion results in a loss in signal from flowing spins.

High-velocity fluid motion through static vessels and arterial branches, such as the carotid bifurcation, produces complex flow patterns, including flow vortices (recirculation) and unsteady, nonrepetitive pulsatile, or turbulent flow. Flow vortices and unsteady, turbulent flow increase phase dispersion of spin coherence due to the multiple directions of motion, acceleration, and higher order motions. Even simple pulsatile flow can result in magnitude and phase signal variations that are a complex function of time. These temporal changes can cause spatial misregistration of pulsatile flow in images. Venous flow is much less pulsatile than arterial flow. Flow velocities in the human body under normal conditions range from a few mm/s up to 180 cm/s.

The phase dispersion among spins having the same constant velocities can be recovered with addition of the gradient waveform lobes known as "flow compensation" or "first-order gradient moment nulling." If the spins are flowing through a gradient $m(G)$, the time-dependent phase of flowing spins (ϕ) at the location r (2.9) is given by

$$\begin{aligned}
&\phi(t) = \int \gamma G(t) \times r(t) \mathrm{d}t \\
&\phi(t) = r_0 \times \int \gamma G(t) \mathrm{d}t + v \times \int \gamma G(t) t \mathrm{d}t + \frac{a}{2} \int \gamma G(t) t^2 \mathrm{d}t + \cdots \\
&\phi(t) = r_0 \times \gamma \times m_0 + v \times \gamma \times m_1 + \frac{a}{2} \times \gamma \times m_2 + \cdots
\end{aligned} \tag{2.9}$$

where the expansion is obtained from a Taylor series expansion of $r(t)$, r_0 is the initial location of the spins, v is the velocity, a is an acceleration of the flow, and m_j is the jth moment of the gradient. Equation (2.9) demonstrates that the behavior of the phase accumulated by the moving spins depends on the initial position, velocity, and gradient strength. If the velocity of each flowing spin is not constant, the phase accumulated after gradient application is not the same for each spin and varies with the velocity. This phase dispersion, if uncorrected, results in signal loss.

To illustrate the effects of velocity on signal phase, an example of RF and gradient waveforms for a conventional SPGR sequence is shown in Fig. 2.3a. Slice selection (SS) is performed by the RF pulse in conjunction with the slice

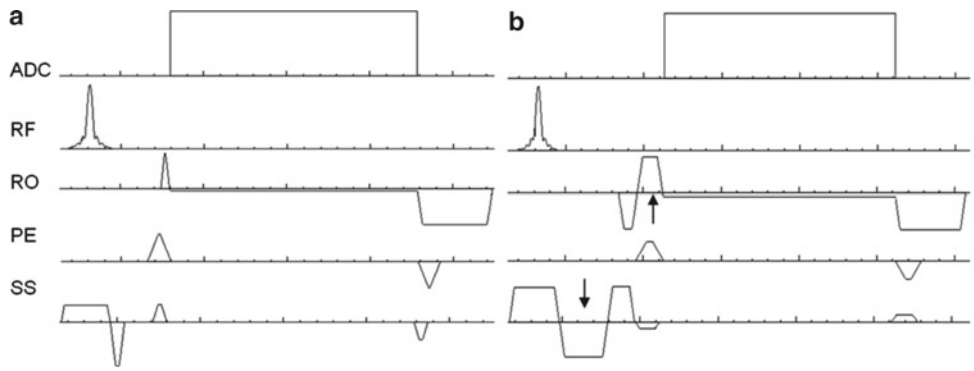

Fig. 2.3 3D SPGR pulse sequence for TOF acquisition without flow compensation (**a**) and with flow compensation in the slice selection and readout direction indicated by *black arrows* (**b**). The abbreviations correspond to data acquisition (ADC), RF pulse (RF), readout (RO) gradient, phase-encoding (PE) gradient, and slice selection (SS) gradient

selection z gradient. The amplitude of the slice selection gradient is determined by the desired slice or slab thickness and the bandwidth of the RF pulse. A refocusing lobe is placed after the end of the RF pulse to compensate for the phase dispersion that occurs after the effective tipping of the magnetization into the transverse plane. The readout (RO) gradient, Gx, that is applied immediately after the RF pulse includes a dephasing lobe prior to signal acquisition so that the received signal is completely in phase at the time, TE, from the RF excitation. The amplitude of the readout gradient is determined by the desired resolution and the readout sampling bandwidth. Finally, a small gradient pulse is applied to the y gradient to create a variation in phase in the y direction during signal readout.

This pulse sequence is repeated and the y gradient is stepped through values from a negative maximum to positive maximum. The SPGR works well for stationary tissues. The zeroth moment, m_0, of both the slice selection and readout gradients is zero at the echo time, TE. The maximum signal occurs for the pulse sequence step, where the y phase-encoding gradient passes through the value, 0. At the time, TE, for this signal measurement, defined as the center of k-space, the stationary spins are completely in phase across the imaging volume. For the signal acquired when the y phase-encoding gradient has zero amplitude, all moments of the y gradient are zero. However, m_1 and the higher gradient moments for the slice selection and readout gradients are not zero at time, TE. Thus, moving spins experience an additional phase shift due to motion during these gradients. Velocity dispersion due to laminar flow results in phase dispersion within a voxel and a net signal loss from flowing spins.

Velocity-dependent phase dispersion can be corrected by a process known as velocity compensation or first-order gradient moment nulling (Fig. 2.3b). This is accomplished by adding additional area, positive and negative, to the gradient pulses used for to the slice selection and readout. The magnitude of the lobes can then be adjusted to ensure that the moments of the waveform, when integrated over time, do not contribute to the velocity-dependent phase dispersion. In other words, flow compensation gradients "null" or zero the effects of phase dispersion. The amplitudes of the two compensation gradient lobes for each gradient are adjusted to null m_0 and m_1 at the times $t = 0$ and $t = \mathrm{TE}$, respectively. In this manner, the phase of stationary and uniformly flowing spins is the same, independent of the velocity of flow velocity.

An additional artifact can occur because of the difference in timing between the phase-encoding and readout gradients. If the time of the phase-encoding gradient is TP, there will be a position shift of $v^*(\mathrm{TE} - \mathrm{TP})$ between the time the "y" coordinate is encoded and the "x" coordinate. Because the image is assumed to be recorded at time, TE, the blood may appear shifted from its actual position at that moment. When the flow is in the readout or phase-encoding direction, the shifted fluid appears to remain within the blood vessel. However, when the flow is diagonal within the readout and phase-encoding plane, the element of fluid appears to shift away from the vessel center with a distance of shift that is proportional to the flow velocity. If the flow is pulsatile, this shift will appear to change in size during the pulse sequence, resulting in blurring and ghosting artifacts. Such artifacts are often seen in the phase-encoding direction originating from the diagonal vessels in the circle of Willis. This last artifact can be eliminated by recognizing that the shift is due to a nonzero, velocity-dependent first moment of the phase-encoding gradient. By adding another lobe to the phase-encoding gradient, it is possible to step m_0 through the values needed for imaging while at the same time nulling m_1 at the time, TE. In 3D TOF, the rephrasing z gradient is usually used as a slice selection phase-encoding gradient. If first-order phase-encoding flow compensation is desired, both extra lobes on the z gradient can be stepped to achieve the desired m_0 while maintaining a zero m_1 at the time, TE.

Due to the additional lobes on the gradient waveforms, the minimum TE is increased. Spins experiencing higher orders of motion, such as constant acceleration, are not compensated by this technique.

Acceleration terms, corresponding to the m_2 moment, occur when flow is pulsatile or changes direction and in this case, some artifacts or signal loss can occur. Usually, this acceleration-caused signal loss is generally quite small and higher order flow compensation is usually not performed. However, it is possible to compensate for phase dispersion induced by constant acceleration by adding an additional lobe to the flow-compensating gradients. This is called second-order gradient motion rephasing or second-order gradient moment nulling, which compensates for constant acceleration. Changes in the rate of acceleration are described as jerk. Jerk can be compensated by third-order gradient moment nulling or third-order gradient motion rephasing with the addition of yet another lobe to the flow-compensating gradients. Signal loss due to these higher order terms is usually much smaller than the loss that would occur from the longer TE required to implement them such that most flow compensation techniques currently in use only compensate for first-order effects from constant velocity flow.

If the TE of the pulse sequence can be made very short, all gradient moments will be small and there is no need for flow compensation. Thus, the phase dispersion in an ultrashort echo time sequence, such as a 3D radial acquisition technique, which requires no slice selection gradients and no readout prephasing, is minimal and there is no need for additional flow compensation [11].

2D TOF

Flow-related enhancement can be reduced by the saturation of signal from the flowing spins, which depends on the number of pulses experienced by the blood, repetition rate, and blood $T1$ recovery time, and by intarvoxel phase dispersion. Saturation effects are important in the setting of slow or in-plane flow, and can be minimized by using thinner slices and relatively long TR. Thus, 2D TOF [12] has the advantage in the setting of slow flow and is often the technique of choice for venous imaging. 2D TOF is also used in evaluation of cervical carotid stenosis to detect slow flow distal to a high-grade stenosis [13]. In 2D TOF imaging, a gradient echo sequence, usually 2D SPGR, is used to sequentially acquire a set of adjacent thin slices, generally 1–3-mm thick. TR, in a range of 20–30 ms, is used with a flip angle of 50–70°. If the velocity of flow is close to the critical velocity of 3–15 cm/s, as given in (2.1), the fluid in each slice experiences only a few RF pulses. The simulation shown in Fig. 2.2 demonstrates that the flow enhancement effect is maximized for flip angle in a range of 50–70°. The short TR and higher flip angle result in enhancement of the contrast between blood and background tissue, as there is insufficient time for longitudinal ($T1$) recovery of the static tissue magnetization and blood flowing into the slice is exposed to only one or two RF pulses for typical arterial velocities of 10–100 cm/s. The imaging plane is generally selected to be perpendicular to the flow direction, such as the axial plane for the carotid arteries. If arterial flow is principally along one axis and venous returns in the opposite direction (such as in the neck, with flow to the brain via the carotid arteries and return via the jugular veins), slice-selective saturation pulses can be used to eliminate the signal from flow in one direction. For example, to eliminate the signal from the jugular veins, a saturation RF pulse is applied superior to the axial slice (Fig. 2.4). To maintain saturation during the acquisition of all slices, this saturation pulse moves together with the axial slice as each subsequent slice is acquired. Blood flowing in the craniocaudal direction in the jugular vein is, thus, saturated before it flows into the imaging slice and produces no signal. Because the saturation pulse distinguishes arteries from veins only by the direction of blood flow, retrograde flow can result in the unwanted saturation of the desired vessel.

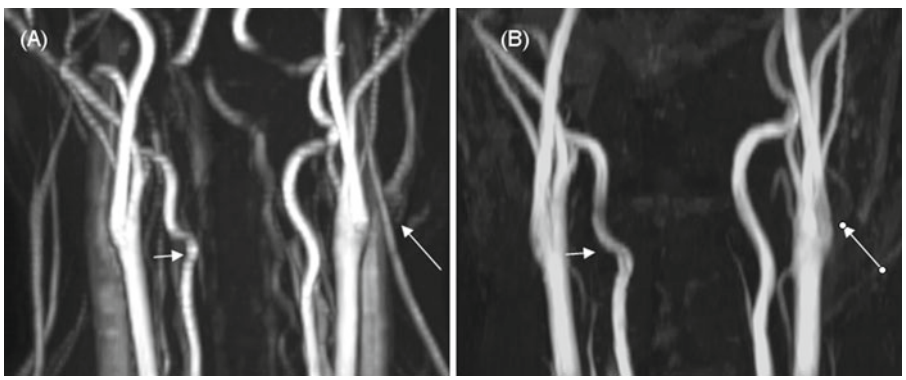

Fig. 2.4 Coronal MIP images of a 2D TOF acquisition of a healthy volunteer using the same acquisition parameters as Fig. 2.3. Coronal MIP image with no spatial saturation pulse (**a**) and with saturation pulse superior to the imaging slices to suppress the venous signal (**b**) (images courtesy of Dr. Tae-Sub Chung, Gangnam Severance Hospital, Seoul, Korea)

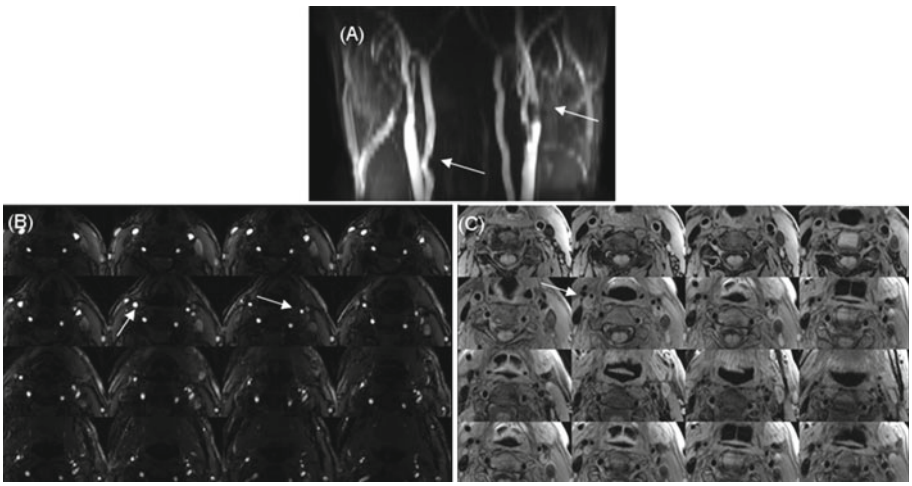

Fig. 2.5 2D TOF acquisition of a patient volunteer with atherosclerosis with TR = 28 ms, TE = 6.7 ms, flip angle = 50°, FOV = 16 cm, matrix = 256 × 256, slice thickness = 3 mm with 20% gap between slices. (**a**) Coronal MIP; (**b**) axial source images; (**c**) 2D black blood T1w images

Transverse (axial) images acquired using 2D TOF in a patient with several severe stenoses just distal to the left and right bifurcation are shown in Fig. 2.5. Black blood 2D *T*1-weighted images (Fig. 2.5c) confirm that atherosclerotic plaque caused the stenosis seen in 2D TOF. Figure 2.5a is obtained as the MIP through the "stack" of acquired image (Fig. 2.5b). Note that MIP images are not true angiograms but rather a projection produced from the source images. Any tissue with a short *T*1 relaxation time such as fat, depending on the exact scan technique used, may be hyperintense in the source images and thus on MIP images they may be potentially confused for flow. Further, the MIP image can be artifactual because only the brightest point along a projection line appears in the MIP image. It is possible that pathology or other important image details are masked behind brighter structures in the MIP image. Thus, when interpreting scans, it is important to review both the MIP and source images. The latter provide a means of assessing surrounding tissues and anatomy and often make identification of artifacts due to motion, signal loss, and the presence of fat easier.

Pulsation and vessel motion induced by pulsation can cause artifacts in 2D TOF imaging. Flow compensation in the slice selection and frequency direction is helpful to reduce the inconsistent phase generated by pulsation [14]. Cardiac triggering can further reduce the artifact induced by pulsation. Fractional echo readout and a tailored excitation RF pulse are used to reduce the TE, since a shorter TE reduces the artifact induced by pulsation. Another drawback of 2D TOF is that complex flow, such as that seen distal to a stenosis, can have high-order motions (acceleration, jerk, etc.) and is not easily compensated for and can result in signal loss. Complex flow patterns specifically lead to signal loss in the region of a stenotic lesion and, thus, overestimation of the degree of stenosis. Although the slice thickness of 2D TOF sequences is usually less than 2 mm, 3D acquisitions can be used to produce images with thinner slices, which, together with the use of shorter TE, reduce the artifactual signal loss [15].

3D TOF

Having intrinsically higher resolution and shorter echo times than 2D TOF, 3D TOF sequences suffer less from intravoxel phase dispersion. In 3D TOF imaging, a single slab of 3D slices is acquired. Like 2D TOF imaging, the slab is oriented to be perpendicular to the direction of flowing blood to ensure good inflow enhancement. SNR and the contrast between in-flowing blood and tissue in 3D TOF depend on the slab thickness and number of slices per slab. The transverse plane is often selected for a carotid or an intracranial 3D TOF acquisition to maximize the inflow enhancement effect; however, an oblique slab orientation is sometimes used, depending on the vessel geometry, to allow the desired imaging volume to be covered with fewer slices, which results in a shorter scan time.

In 3D TOF acquisition, the blood inside the imaging slab generally experiences multiple RF pulses, so a smaller flip angle compared to that in 2D TOF is used to maximize the inflow enhancement effect. Further, spatial saturation is not usually applied in 3D TOF. Although spatial saturation could be applied in 3D TOF acquisition, it would increase the minimum TR and the venous signal in 3D TOF is already suppressed, except on a few entry slices, by the slow venous flow and thicker slab. Short TRs (~20 ms) in 3D TOF also result in reduced contrast between flowing and stationary tissue, including muscle and fat, which generally have a short *T*1 relaxation time compared with blood. Magnetization

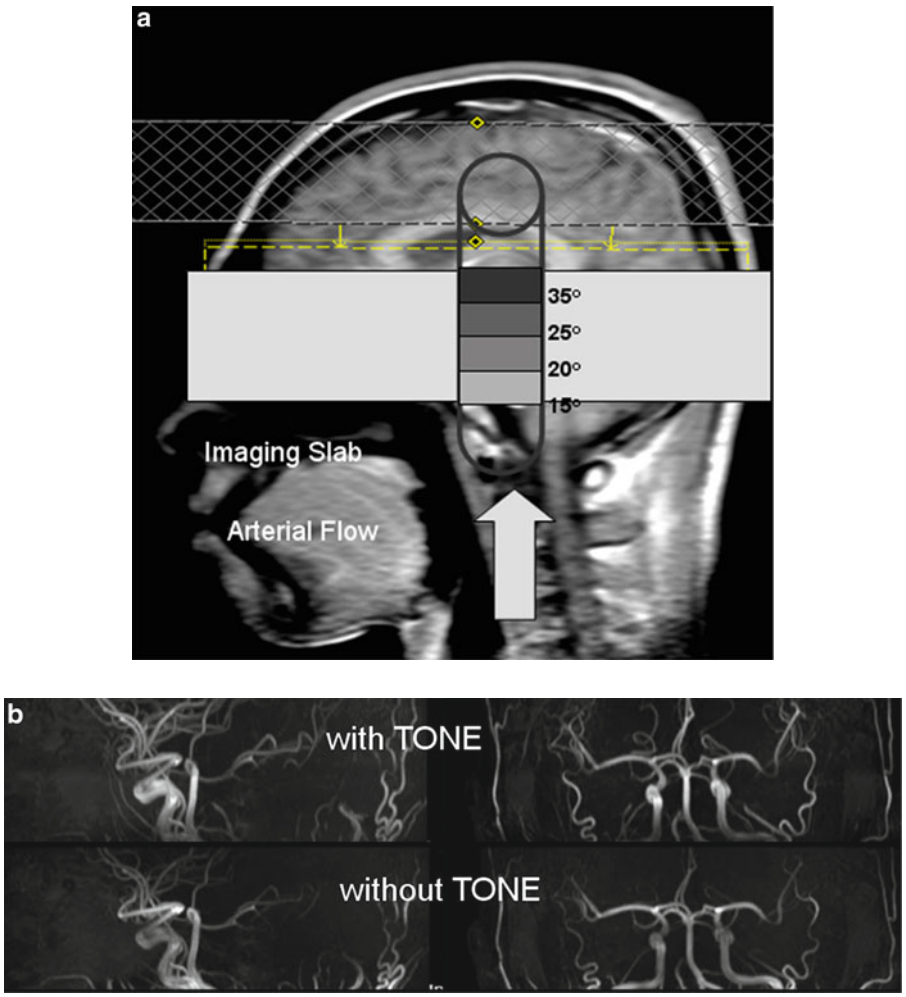

Fig. 2.6 (**a**) Schematic representation of TONE pulse. The flip angle of the TONE pulse increases as a function of distance in order to equalize the signal from flowing blood (indicated by *arrow*). (**b**) Coronal and sagittal MIP of 3D TOF acquisition of a volunteer at 1.5 T with and without TONE technique. The MIP image constructed with TONE shows the uniform vessel signal around edge (images courtesy of Dr. Tae-Sub Chung, Gangnam Severance Hospital, Seoul, Korea)

transfer is often used in 3D TOF to suppress the signal from the stationary tissue and to increase further the contrast between the flow and tissue. To minimize artifacts induced by turbulent or pulsatile flow, the echo time in 3D TOF is made as short as possible. Fractional echo readout and a short duration or asymmetric RF excitation pulse are used to achieve the shortest possible echo time. For situations where the signal from lipid can be a problem, an echo time can be selected, where the signal from lipid and water is out of phase, yielding better contrast between the two at the expense of a slight increase in problems due to the longer echo time. This out-of-phase echo time varies with the magnet field strength.

When imaging with a thick 3D slab, the number of pulses experienced by the blood increases with distance into the slab. RF excitation that is uniform across the 3D slab results in greater inflow enhancement where the blood enters the slab, whereas distal slices in which blood has experienced more RF pulses experience less flow enhancement signal. To compensate for the resulting variation in signal saturation, it has been found useful to make the RF excitation tip angle be a function of distance into the slab. For example, ramped RF excitation, where the tip angle is small at the slab entrance and increases with distance into the slab, is commonly used for 3D TOF to make the flowing blood signal across the imaging slab as uniform as possible [6, 16]. Ramped RF pulses, with spatially varying flip angle profiles parallel to the direction of flow, are often called tilted optimized non-saturating excitation (TONE) pulses (Fig. 2.6).

A variety of different flow compensation strategies are used in 3D TOF. Generally, flow compensation on the readout and slab selection gradient is used. In this case, the individual phase-encoding steps in the slice and phase-encoding gradient are not compensated. As described above, phase-encoding flow compensation can be used to compensate each step of both phase-encoding gradient waveforms. Although,

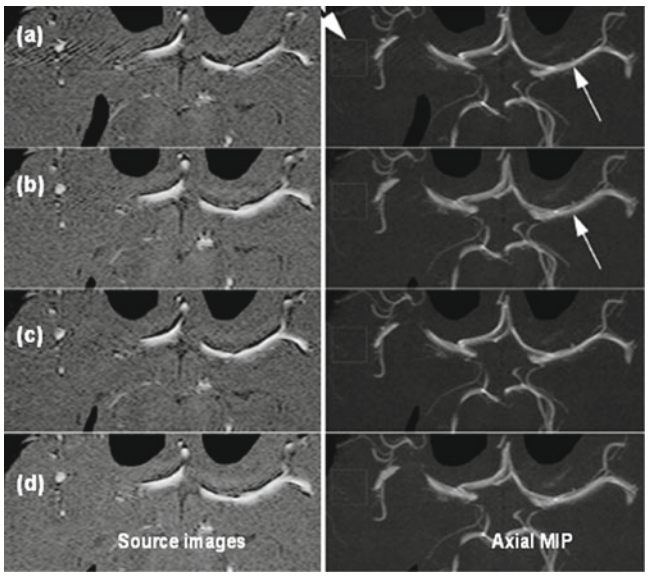

Fig. 2.7 Images obtained from four types of acquisition, from top to bottom. **a–b,** linear view ordering with (**a**) slice selection/frequency-encoding flow compensation and (**b**) three-directional flow compensation (3DFC). **c–d,** centric view ordering with (**c**) slice selection/frequency-encoding flow compensation and (**d**) 3DFC. The cross-hatch artifacts arising from blood flow pulsations in the source images and other vessels near the circle of Willis are clearly evident in the two images in the *top row*. The artifacts are reduced by both 3DFC (*second row of axial images*) and centric view ordering acquisition order (*third row*), and the greatest reduction is observed when 3DFC is combined with centric view ordering acquisition (*bottom row*). More importantly, from the MIP images (*right column*), we note the change in apparent lumen diameter of the M1 segment (*arrow*) when using 3DFC. Without 3DFC, the obliquely oriented vessels have bright rims that are consistent with distortion or signal "pileup" (from Parker et al. [17], with permission)

such phase-encoding flow compensation generally results in an increased echo time, it has the advantage of eliminating the misregistration artifact if blood is flowing obliquely to the frequency-encoding and one or both of the phase-encoding gradients (Fig. 2.7) [17]. To reduce the echo time in high-resolution 3D TOF acquisition with three-direction flow compensation, a variable TE technique has been introduced [18, 19]. A variable TE technique in 3D TOF with three-direction flow compensation can minimize the TE at the center of *k* space. In this technique, *k* space of the 3D TOF is divided into several segments with different TE. Flow-compensation gradient lobes are calculated for each segment and the echo time at each segment is minimized. This results in a shorter echo time at the center of *k* space and a reduced flow-related signal void due to long echo times.

k-Space Sampling Strategies

3D MRA acquired using ultrashort TE sequences, such as projection or spiral acquisition, gives a minimal artifact from phase dispersion of flow across a voxel, even without flow

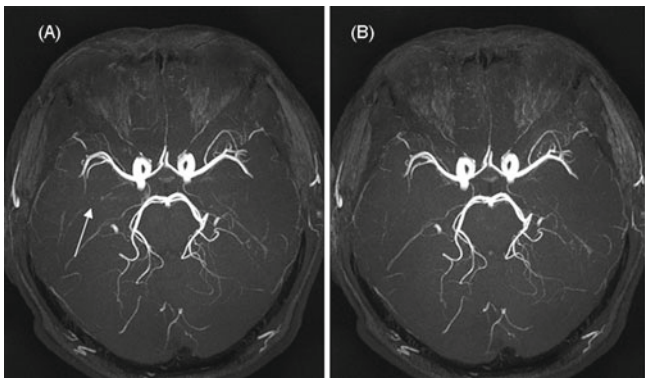

Fig. 2.8 Axial MIP of 3D TOF acquisition of a healthy volunteer at 3.0 T (**a**) with linear view order and (**b**) with centric view order. Notice that the ghost artifact caused by pulsatile flow that propagates in the primary phase-encoding direction is reduced when centric view order is used

compensation [20–22]. Ultrashort TE pulse sequences are also useful for scanning the brain in the presence of a metal clip or stent. In a 3D TOF acquisition, the order of *k*-space acquisition can be rearranged to reduce the prominence of artifacts induced by pulsatile flow (Fig. 2.8). A linear view order acquisition generally causes ghosts that are dominant along the phase-encoding direction [23]. An elliptical centric view order acquisition, which acquires the centric *k*-space first, spreads the ghosts evenly in the phase- and slice-encoding directions.

Magnetization Transfer

3D TOF with magnetization transfer has been employed for intracranial MRA to suppress the signal intensity of background brain tissue [24]. An MT pulse is a spectrally selective RF pulse that reduces the signal from tissue that has higher amounts of large molecules. Water molecules that are in contact with macromolecules generally move slowly and have a broad NMR resonance. Off-resonant excitation can saturate the magnetization on these water molecules. When these water molecules exchange with free water, the net magnetization in the tissue is reduced. Because blood has a lower concentration of macromolecules, off-resonance MT pulses can be used to selectively saturate the magnetization in station tissues with minimal effect on blood magnetization. In 3D TOF, MT is used to suppress the signal intensity of the brain parenchyma while leaving the signal from blood unaffected, thus improving smaller vessel visibility. Figure 2.9 shows a comparison of intracranial 3D TOF images acquired without and with the inclusion of MT pulses.

An MT RF pulse generally requires a long pulse duration and higher RF power. Thus, MT pulse application causes increased TR and further increases the already long scan time of high-resolution 3D TOF acquisition. To increase the time

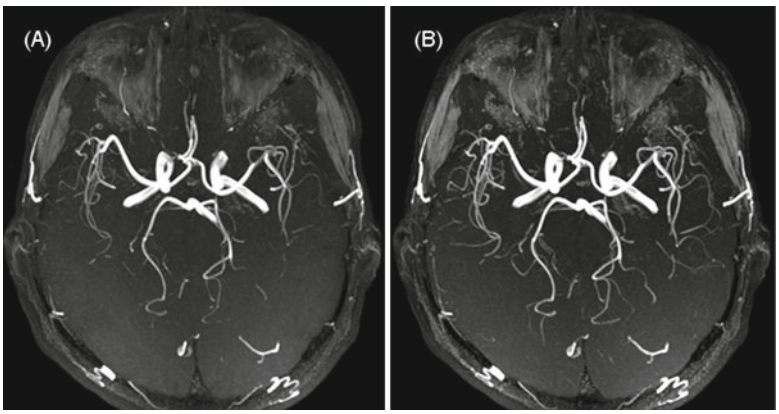

Fig. 2.9 Axial MIP of 3D TOF acquisition of a volunteer at 1.5 T (**a**) without MT saturation and (**b**) with MT saturation. Notice that MIP with MT saturation demonstrates more small, distal, middle cerebral arteries' detections (images courtesy of Dr. Tae-Sub Chung, Gangnam Severance Hospital, Seoul, Korea)

efficiency in 3D TOF, the majority of the MT effect is obtained by applying the MT pulses only around the center of *k*-space [25]. The use of MT saturation at high field strength becomes problematic because the SAR increases with the square of the RF transmission frequency, which is proportional to the main magnetic field strength. For this reason, MT saturation in TOF has been utilized only at 1.5 or 3.0 T.

Because of the chemical shift between the fat and water, there is a small (3 ppm) difference in Larmor frequency between fat and water resonances, and a TE-dependent phase shift in their signal contributions to a given voxel. Choosing a TE at which fat and water are outphase can provide some fat suppression. However, the TE, where water and fat are out of phase, is greater than the minimum TE achieved by the pulse sequence and further increases the signal loss induced by intravoxel phase dispersion. As a general rule, the TE should be minimized at the cost of other considerations because of the rapid increase in intravoxel diphase dispersion that accompanies increased TE.

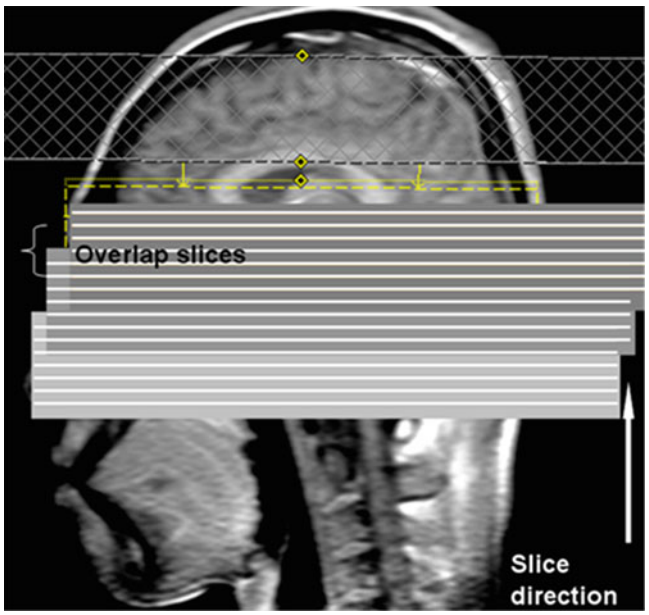

Fig. 2.10 Schematic representation of a MOTSA acquisition with three slabs and eight slices per slab. There are three overlap slices at each boundary between slabs

Multiple Overlapping Thin 3D Slab Acquisition

3D TOF MRA is susceptible to signal loss due to saturation of the moving spins in thick slabs. To reduce flow signal saturation while retaining the high spatial resolution, short echo times, and some of the SNR advantages of 3D techniques, a sequential acquisition of multiple 3D slabs has been developed. MOTSA has all the advantages of the single-volume 3D TOF techniques, and the use of overlapping thin slabs generally overcomes the problem of spin saturation. MOTSA is currently one of the most popular clinical 3D TOF applications [4]. This popularity is due in part to stronger in-flow enhancement and better vessel contrast-to-noise ratio properties of MOTSA compared to other techniques. Multiple thin slab acquisition reduces the signal saturation of slowly flowing blood compared to one thick single-slab acquisition, and overlapping slab acquisition eliminates the signal void from each slab boundary region – often called the venetian blind artifact. The slices located in the overlapped region can be acquired twice with an entry slice from the first slab and an exit slice from the next slab [26]. This technique moderates the variation of the final MIP image intensity after taking the maximum of two images using a pixel-by-pixel comparison. Increasing the amount of slab overlap can obviously reduce the slab boundary artifact. Using a slab overlap of 50% can almost completely eliminate the artifact (Fig. 2.10). However, increasing overlap also increases the scan time per unit coverage in the slice direction. A sliding interleaved *ky* (SLINKY) sequence was proposed as an alternative technique to reduce the slab boundary artifact in multiple slab acquisition [27]. In a typical MOSTA data acquisition, the slab excitation is shifted

after acquisition of all of *ky* and *kz* phase encodings. In SLINKY acquisition, the slab excitation is sliding every few views by one slab location. A designated partial set of the *ky* phase-encoding steps are collected and the acquisition of the partial set of the *ky* space is interleaved during continuous sliding of a slab along the slice selection direction [28]. SLINKY equalizes the flow enhancement effect across the entire slab dimension and eliminates the slab boundary artifacts while retaining good acquisition time efficiency compared with conventional MOTSA.

TOF at High Magnetic Fields

3D TOF MRA is considered to be a safe, fully noninvasive imaging procedure with submillimeter spatial resolution. As such, it is routinely used to screen for cerebrovascular diseases, such as aneurysms and arteriovenous malformations. However, more subtle microvascular disease usually cannot be seen with the resolution capabilities of standard field strength MRA. Increased vessel contrast and spatial resolution are highly desirable for more sensitive detection of small aneurysms and vasculitis and for improved morphological characterization of larger aneurysms. The recent development of ultrahigh-field MRI scanners enables assessment of the cerebral arteries with a spatial resolution previously not achieved with standard MRI scanners. MRA at 7.0 T has shown superior contrast between blood and background tissue mainly because of the increased *T*1 recovery time of tissues and better suppression of the background signal relative to that of the blood vessels [29]. The increased SNR also yields improved visualization of the microvasculature of the human brain at high spatial resolution [30] (Fig. 2.11).

However, at very high field strengths, the frequency-encoding dimension is limited by the TE-dependent artifacts of susceptibility-induced dephasing and pulsatile flow, and the extended scan time needed for phase encoding of the larger matrix is not clinically feasible. Parallel imaging (PI) techniques can accelerate scans at the cost of SNR and, thus, can achieve very-high-resolution MRA studies within a reasonable scan time [31]. For example, optimized coils coupled with PI techniques at 3.0 T can yield scan times similar to or shorter than those at 1.5 T. On this basis, intracranial TOF image quality improvements have previously been described in the transition from 1.5 to 3 T and 3 to even 7 T [32].

Summary

In this discussion, we have presented a general overview of the basics of TOF MRA and provided discussion of the various trade-offs in image acquisition. Many of the concepts of TOF MRA were developed in the late 1980s and early 1990s, and hence are very mature. However, improvements in MRI techniques and technology have also led to progress in TOF MRA. These improvements include improved gradient capabilities, higher magnetic field strength, increased number and quality of RF channels and components, and new pulse sequences and acquisition techniques. In the past 20 years, gradient performance has increased from 1 mT/m and 20 T/m/s to over 40 mT/m and 200 T/m/s. Field strength in clinically used MRI scanners has now reached 3 T, and work is being performed at 7 T. The number of receiver channels has increased from 1 to as many as 128 on commercially available scanners, allowing the design of receiver coil arrays with more elements to allow parallel imaging to reduce image acquisition time and thereby reduce motion artifacts. Finally, new pulse sequences, including 3D radial acquisition, PROPELLER, and many others, have increased the flexibility available for novel TOF MRA techniques. Thus, as it is with many fields of MRI, TOF MRA continues to evolve in capability and ultimate utility.

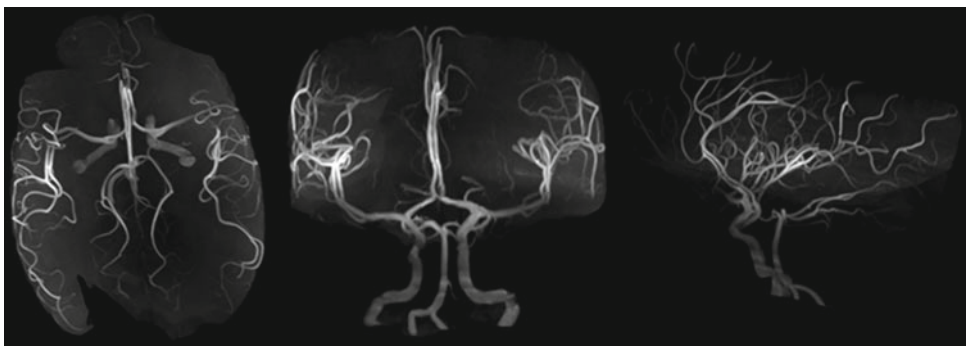

Fig. 2.11 TOF MRA acquired at 7 T with a custom-built transmit/receive head coil with eight stripline elements. TR/TE 21/3.4 ms; flip angle 40°; bandwidth 303 Hz/pixel; resolution $0.6 \times 0.5 \times 0.6$ mm^3 (non-interpolated); acquisition time 5 min 58 s; parallel imaging with GRAPPA, reduction factor 2, 40 reference lines. The high spatial resolution enables nice depiction of fine, peripheral vessels (images courtesy of Mark Ladd of the Erwin L. Hahn Institute for MRI, Essen, Germany)

References

1. Suryan G. A time-of-flight method. *Proc Indian Acad Sci Sect.* 1959;A33:107.
2. Hinshaw WS, Bottomley PA, Holland GN. Radiographic thin section image of the human wrist by nuclear magnetic resonance. *Nature.* 1977;270:272–273.
3. Laub G. Displays for MR angiography. *Magn Reson Med.* 1990;14:222–229.
4. Parker DL, Yuan C, Blatter DD. MR angiography by multiple thin slab 3D acquisition. *Magn Reson Med.* 1991;17:434–451.
5. Davis WL, Warnock SH, Harnsberger HR, Parker DL, Chen CX. Intracranial MRA: single volume vs. multiple thin slab 3D time-of-flight acquisition. *J Comput Assist Tomogr.* 1993;17:15–21.
6. Atkinson D, Brant-Zawadzki M, Gillan G, Purdy D, Laub G. Improved MR angiography: magnetization transfer suppression with variable flip angle excitation and increased resolution. *Radiology.* 1994;190:890–894.
7. Axel L, Shimakawa A, MacFall J. A time-of-flight method of measuring flow velocity by magnetic resonance imaging. *Magn Reson Imaging.* 1986;4:199–205.
8. Gullberg GT, Wehrli FW, Shimakawa A, Simons MA. MR vascular imaging with a fast gradient refocusing pulse sequence and reformatted images from transaxial sections. *Radiology.* 1987;165: 241–246.
9. Nishimura DG. Time-of-flight MR angiography. *Magn Reson Med.* 1990;14:194–201.
10. Vlaardingerbroek, MT, den Boer JA. *Magnetic Resonance Imaging: Theory and Practice*. Springer Verlag Telos; 1996:191–204.
11. Nielsen HT, Gold GE, Olcott EW, Pauly JM, Nishimura DG. Ultrashort echo-time 2D time-of-flight MR angiography using a half-pulse excitation. *Magn Reson Med.* 1999;41:591–599.
12. Keller PJ, Drayer BP, Fram EK, Williams KD, Dumoulin CL, Souza SP. MR angiography with two-dimensional acquisition and three-dimensional display. Work in progress. *Radiology.* 1989;173: 527–532.
13. Heiserman JE, Drayer BP, Fram EK, et al. Carotid artery stenosis: clinical efficacy of two-dimensional time-of-flight MR angiography. *Radiology.* 1992;182:761–768.
14. Urchuk SN, Plewes DB. Mechanisms of flow-induced signal loss in MR angiography. *J Magn Reson Imaging.* 1992;2:453–462.
15. Keller PJ. Magnetic resonance angiography of the neck. Technical issues. *Neuroimaging Clin N Am.* 1996; 6:853–861.
16. Priatna A, Paschal CB. Variable-angle uniform signal excitation (VUSE) for three-dimensional time-of-flight MR angiography. *J Magn Reson Imaging.* 1995;5:421–427.
17. Parker DL, Goodrick KC, Roberts JA, et al. The need for phase-encoding flow compensation in high-resolution intracranial magnetic resonance angiography. *J Magn Reson Imaging.* 2003;18: 121–127.
18. Song HK, Wehrli FW. Variable TE gradient and spin echo sequences for in vivo MR microscopy of short T2 species. *Magn Reson Med.* 1998;39:251–258.
19. Jeong EK, Parker DL, Tsuruda JS, Won JY. Reduction of flow-related signal loss in flow-compensated 3D TOF MR angiography, using variable echo time (3D TOF-VTE). *Magn Reson Med.* 2002;48:667–676.
20. Schmalbrock P, Yuan C, Chakeres DW, Kohli J, Pelc NJ. Volume MR angiography: methods to achieve very short echo times. *Radiology.* 1990;175:861–865.
21. Glover GH, Lee AT. Motion artifacts in fMRI: comparison of 2DFT with PR and spiral scan methods. *Magn Reson Med.* 1995;33: 624–635.
22. Glover GH, Pauly MJ. Projection reconstruction techniques for reduction of motion effects in MRI. *Magn Reson Med.* 1992; 28:275–289.
23. Wilman AH, Riederer SJ, King BF, et al. Fluoroscopically triggered contrast-enhanced three-dimensional MR angiography with elliptical centric view order: application to the renal arteries. *Radiology*. 1997;205:137–146.
24. Dagirmanjian A, Ross JS, Obuchowski N, et al. High resolution, magnetization transfer saturation, variable flip angle, time-of-flight MRA in the detection of intracranial vascular stenoses. *J Comput Assist Tomogr*. 1995;19:700–706.
25. Parker DL, Buswell HR, Goodrich KC, Alexander AL, Keck N, Tsuruda JS. The application of magnetization transfer to MR angiography with reduced total power. *Magn Reson Med*. 1995;34: 283–286.
26. Blatter DD, Bahr AL, Parker DL, et al. Cervical carotid MR angiography with multiple overlapping thin-slab acquisition: comparison with conventional angiography. *AJR Am J Roentgenol*. 1993;161:1269–1277.
27. Liu K, Rutt BK. Sliding interleaved kY (SLINKY) acquisition: a novel 3D MRA technique with suppressed slab boundary artifact. *J Magn Reson Imaging*. 1998;8:903–911.
28. Liu K, Lee DH, Rutt BK. Systematic assessment and evaluation of sliding interleaved kY (SLINKY) acquisition for 3D MRA. *J Magn Reson Imaging*. 1998;8:912–923.
29. Kang CK, Park CW, Han JY, et al. Imaging and analysis of lenticulostriate arteries using 7.0-Tesla magnetic resonance angiography. *Magn Reson Med*. 2009;61:136–144.
30. Kang CK, Hong SM, Han JY, et al. Evaluation of MR angiography at 7.0 Tesla MRI using birdcage radio frequency coils with end caps. *Magn Reson Med*. 2008;60:330–338.
31. von Morze C, Purcell DD, Banerjee S, et al. High-resolution intracranial MRA at 7T using autocalibrating parallel imaging: initial experience in vascular disease patients. *Magn Reson Imaging*. 2008;26:1329–1333.
32. von Morze C, Xu D, Purcell DD, et al. Intracranial time-of-flight MR angiography at 7T with comparison to 3T. *J Magn Reson Imaging*. 2007;26:900–904.

http://www.springer.com/978-1-4419-1685-3

Magnetic Resonance Angiography
Principles and Applications
Carr, J.C.; Carroll, T.J. (Eds.)
2012, XVII, 412 p., Hardcover
ISBN: 978-1-4419-1685-3